

## Accepted Manuscript

### Macrocyclic Inhibitors of Factor XIa: Discovery of Alkyl-Substituted Macrocyclic Amide Linkers with Improved Potency

James R. Corte, Wu Yang, Tianan Fang, Yufeng Wang, Honey Osuna, Amy Lai, William R. Ewing, Karen A. Rossi, Joseph E. Myers Jr., Steven Sheriff, Zhen Lou, Joanna J. Zheng, Timothy W. Harper, Jeffrey M. Bozarth, Yiming Wu, Joseph M. Luetzgen, Dietmar A. Seiffert, Mimi L. Quan, Ruth R. Wexler, Patrick Y.S. Lam

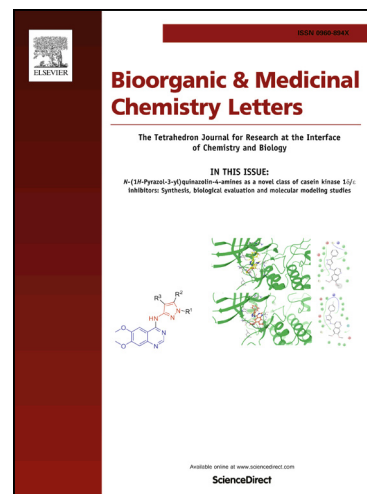
PII: S0960-894X(17)30660-1  
DOI: <http://dx.doi.org/10.1016/j.bmcl.2017.06.058>  
Reference: BMCL 25092

To appear in: *Bioorganic & Medicinal Chemistry Letters*

Received Date: 2 May 2017  
Accepted Date: 21 June 2017

Please cite this article as: Corte, J.R., Yang, W., Fang, T., Wang, Y., Osuna, H., Lai, A., Ewing, W.R., Rossi, K.A., Myers, J.E. Jr., Sheriff, S., Lou, Z., Zheng, J.J., Harper, T.W., Bozarth, J.M., Wu, Y., Luetzgen, J.M., Seiffert, D.A., Quan, M.L., Wexler, R.R., Lam, P.Y.S., Macrocyclic Inhibitors of Factor XIa: Discovery of Alkyl-Substituted Macrocyclic Amide Linkers with Improved Potency, *Bioorganic & Medicinal Chemistry Letters* (2017), doi: <http://dx.doi.org/10.1016/j.bmcl.2017.06.058>

This is a PDF file of an unedited manuscript that has been accepted for publication. As a service to our customers we are providing this early version of the manuscript. The manuscript will undergo copyediting, typesetting, and review of the resulting proof before it is published in its final form. Please note that during the production process errors may be discovered which could affect the content, and all legal disclaimers that apply to the journal pertain.





## Macrocyclic Inhibitors of Factor XIa: Discovery of Alkyl-Substituted Macrocyclic Amide Linkers with Improved Potency.

James R. Corte<sup>a,\*</sup>, Wu Yang<sup>a,\*</sup>, Tianan Fang<sup>a</sup>, Yufeng Wang<sup>a</sup>, Honey Osuna<sup>a</sup>, Amy Lai<sup>a</sup>, William R. Ewing<sup>a</sup>, Karen A. Rossi<sup>a</sup>, Joseph E. Myers Jr.<sup>b</sup>, Steven Sheriff<sup>b</sup>, Zhen Lou<sup>c</sup>, Joanna J. Zheng<sup>c</sup>, Timothy W. Harper<sup>c</sup>, Jeffrey M. Bozarth<sup>c</sup>, Yiming Wu<sup>c</sup>, Joseph M. Luetzgen<sup>c</sup>, Dietmar A. Seiffert<sup>c</sup>, Mimi L. Quan<sup>a</sup>, Ruth R. Wexler<sup>a</sup> and Patrick Y. S. Lam<sup>a</sup>

<sup>a</sup>Bristol-Myers Squibb Company, Research and Development, 350 Carter Road, Hopewell, New Jersey 08540, United States

<sup>b</sup>Bristol-Myers Squibb Company, Research and Development, US Rt. 206 & Province Line Road, Princeton, New Jersey 08540, United States

<sup>c</sup>Bristol-Myers Squibb Company, Research and Development, 311 Pennington-Rocky Hill Road, Pennington, New Jersey 08543-2130, United States

### ARTICLE INFO

#### Article history:

Received  
Revised  
Accepted  
Available online

#### Keywords:

Factor XIa inhibitors  
FXIa  
Activated Partial Thromboplastin Time  
aPTT  
Thrombosis

### ABSTRACT

Optimization of macrocyclic inhibitors of FXIa is described which focused on modifications to both the macrocyclic linker and the P1 group. Increases in potency were discovered through interactions with a key hydrophobic region near the S1 prime pocket by substitution of the macrocyclic linker with small alkyl groups. Both the position of substitution and the absolute stereochemistry of the alkyl groups on the macrocyclic linker which led to improved potency varied depending on the ring size of the macrocycle. Replacement of the chlorophenyltetrazole cinnamide P1 in these optimized macrocycles reduced the polar surface area and improved the oral bioavailability for the series, albeit at the cost of a decrease in potency. ©2014 Elsevier Science Ltd. All rights reserved.

\* Corresponding author. Tel.: +1-609-466-5030; fax: +1-609-818-3331; e-mail: james.corte@bms.com

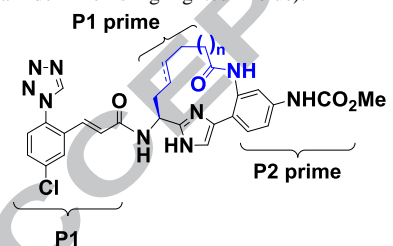
\* Corresponding author. Tel.: +1-609-466-5100; fax: +1-609-818-3331; e-mail: wu.yang@bms.com

Novel oral anticoagulants (NOACs), such as the direct thrombin inhibitor (dabigatran) and direct Factor Xa inhibitors (rivaroxaban, apixaban, and edoxaban), are effective for the prevention and treatment of deep vein thrombosis (DVT) and pulmonary embolism, and stroke prevention in non-valvular atrial fibrillation.<sup>1</sup> Rivaroxaban is also effective for the secondary prevention of acute coronary syndrome (ACS), however an increased risk of bleeding and intracranial hemorrhage was observed.<sup>2,3</sup> Safer and more efficacious anticoagulants remains a medical need.

Based on the lack of an overt bleeding phenotype for individuals with a genetic FXI deficiency (Hemophilia C), inhibition of the blood coagulation enzyme Factor XIa (FXIa), the activated form of the zymogen Factor XI (FXI), could provide an effective anticoagulant therapy with a safer bleeding profile.<sup>4</sup> Individuals with severe FXI deficiency appear to be protected from certain cardiovascular events as they show reduced rates of both ischemic stroke and DVT.<sup>5</sup> Importantly, from a safety perspective, the majority of individuals with Hemophilia C display a minor bleeding tendency which is in contrast to the bleeding episodes observed with either a severe Factor VIII deficiency (Hemophilia A) or a severe Factor IX deficiency (Hemophilia B).<sup>6</sup>

Several FXIa inhibitors, such as  $\alpha$ -ketothiazole peptidomimetic,<sup>7</sup> 4-carboxy-2-azetidinone,<sup>8</sup> tetrahydroquinoline,<sup>9</sup> and chloroimidazole derivatives,<sup>10</sup> were shown to be effective in a variety of animal thrombosis models with minimal effects on bleeding time. Moreover, we have shown that at equivalent antithrombotic doses, a tetrahydroquinoline FXIa inhibitor displayed less bleeding in a rabbit cuticle bleeding time model when compared to the direct thrombin inhibitor dabigatran.<sup>9b</sup> These preclinical studies support targeting FXIa as a means to achieve greater protection from thrombosis without increasing the bleeding risk.

**Table 1.** 12- and 13-membered macrocyclic FXIa inhibitors (the macrocyclic amide linker is highlighted in blue).



Compd #	n (ring size)	Alkene	FXIa Ki (nM) <sup>12</sup>	aPTT EC <sub>1.5x</sub> ( $\mu$ M) <sup>13</sup>
1	0 (12)	saturated	1.0	0.30
2	1 (13)	saturated	3.2	1.2
3	1 (13)	E-alkene	0.16	0.27

We recently disclosed the discovery of a novel series of 12- and 13-membered macrocyclic FXIa inhibitors **1-3** (Table 1).<sup>11</sup> The macrocyclic amide linker, highlighted in blue, was critical for FXIa binding affinity. The presence of the E-alkene in the 13-membered amide-linker **3** reduced the conformational entropy and showed improved FXIa affinity

compared to either the 12- or 13-membered saturated amide linkers **1** or **2**. Importantly, these amide-linked macrocycles exhibited excellent *in vitro* anticoagulant activity as measured by an activated partial thromboplastin time (aPTT) clotting assay ( $EC_{1.5x} = 0.27-1.2 \mu\text{M}$ ).<sup>13</sup> However, this macrocyclic series suffered from poor oral bioavailability as illustrated below for compounds **1-3**, most likely due to low permeability arising from high polar surface area (PSA = 169  $\text{\AA}^2$  for macrocycles **1-3**).<sup>14</sup> Our optimization strategy for the macrocyclic series was two-fold. First, we wanted to probe the S1 prime pocket with modifications to the unexplored alkyl backbone portion of the macrocyclic linker with the goal of enhancing potency. Second, we sought to address the poor oral bioavailability for the series by improving the permeability via reduction of PSA. In this communication, we describe the discovery of alkyl-substituted macrocycles with improved FXIa affinity as well as our initial efforts to improve oral bioavailability for the series by replacing chlorophenyltetrazole cinnamide (**P1**) with a smaller, less polar group.

X-ray crystallography of macrocycles **1** and **2** confirmed a key hydrogen bond, which had been suggested by molecular modeling, between the NH of the amide moiety in the macrocyclic linker and the carbonyl of Leu41 in FXIa resulting in a significant increase in FXIa affinity.<sup>11,15</sup> The crystal structures also revealed that the alkyl backbone of the macrocyclic amide linker did not fully access the hydrophobic region, represented by the yellow surface in the S1 prime pocket (Figure 1).<sup>16</sup> Owing to the fact that additional potency enhancements might be achievable by targeting this hydrophobic region, we explored alkyl substitutions on the linker in both the 12- and 13-membered macrocycles.

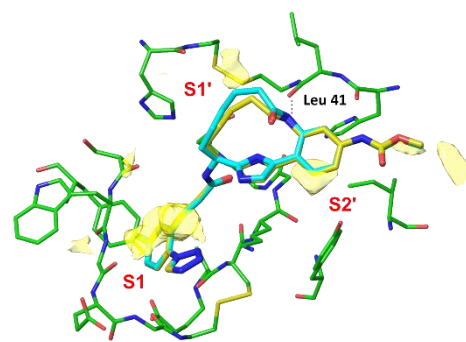
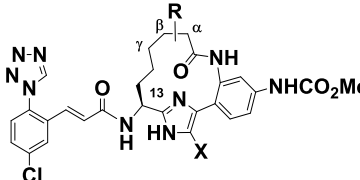


**Figure 1.** Overlay of X-ray structures of **1** (yellow) and **2** (cyan) in FXIa. Yellow surfaces highlight key hydrophobic regions within the FXIa binding site as determined by SiteMap.<sup>16</sup>

We initially explored methyl substitution at the  $\alpha$ -,  $\beta$ -, and  $\gamma$ -positions in the 13-membered saturated linker (Table 2). Compound **2** and its corresponding chloroimidazole analog **4** were included for comparison. From our previously disclosed SAR, adding a chloro group to the 5 position of the imidazole generally provides a 5-fold increase in FXIa affinity and the chloroimidazole scaffold is a common structural motif in our more potent macrocyclic analogs.<sup>11,17</sup> Substitution at the  $\alpha$ -position relative to the amide resulted in a loss in FXIa affinity and aPTT activity for both diastereomers **5** and **6**. The stereochemistry of a methyl group at the  $\beta$ -position had a more dramatic effect on FXIa

affinity. Whereas diastereomer (*R*)- $\beta$ -Me **7** exhibited a 6- to 7-fold loss in FXIa affinity, the corresponding diastereomer (*S*)- $\beta$ -Me **8**<sup>18</sup> exhibited a 4.5-fold increase in FXIa affinity compared to the unsubstituted analog **2**. In spite of the improvement in FXIa affinity, the potency in the aPTT clotting assay was unchanged. The lack of change in the aPTT clotting assay is likely at least in part due to higher protein binding with the installation of the methyl group [human protein binding (%bound) for **2** is 96.2% and **8** is 98.0%]. Incorporation of the (*S*)- $\beta$ -Me group in chloroimidazole **9** resulted in an 8-fold improvement in FXIa affinity (FXIa  $K_i$  = 0.06 nM), however only a modest increase in aPTT activity was observed (compare **4** vs **9**). Substitution at the  $\gamma$ -position led to a loss in FXIa affinity and aPTT activity for both diastereomers **10** and **11**. In summary, a  $\beta$ -methyl group improved FXIa affinity in the 13-membered saturated linker.

**Table 2.** Substitutions on the 13-membered saturated macrocyclic linker



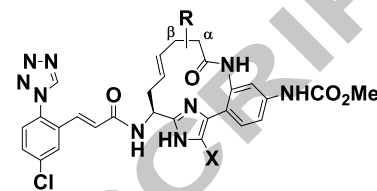
Compd #	R	X	FXIa $K_i$ (nM) <sup>12</sup>	aPTT $EC_{1.5x}$ ( $\mu$ M) <sup>13</sup>
<b>2</b>	H	H	3.2	1.2
<b>4</b>	H	Cl	0.47	0.92
<b>5</b> <sup>a</sup> (diastereomer A)	$\alpha$ -Me	H	6.5	5.3
<b>6</b> <sup>a</sup> (diastereomer B)	$\alpha$ -Me	H	31	32
<b>7</b> <sup>a</sup>	( <i>R</i> )- $\beta$ -Me <sup>b</sup>	H	21	27
<b>8</b> <sup>a</sup>	( <i>S</i> )- $\beta$ -Me <sup>b</sup>	H	0.69	1.1
<b>9</b>	( <i>S</i> )- $\beta$ -Me <sup>b</sup>	Cl	0.06	0.57
<b>10</b> <sup>a</sup> (diastereomer A)	$\gamma$ -Me	H	5.9	2.5
<b>11</b> <sup>a</sup> (diastereomer B)	$\gamma$ -Me	H	18	12

<sup>a</sup>All diastereomers were separated. The diastereomeric excess for **5** was 91% de, **6** was  $\geq$  95% de, **10** was 79% de, and **11** was 89% de as determined by <sup>1</sup>H NMR. The diastereomeric excess of **7** and **8** were  $\geq$  99% de as determined by analytical chiral hplc. <sup>b</sup>The absolute stereochemistry was assigned based on an X-ray co-crystal of **8** with FXIa (Figure 2A).

Since a  $\beta$ -methyl group improved FXIa affinity in the 13-membered saturated linker, it was installed in the 13-membered unsaturated linker (Table 3). The unsubstituted amide linkers containing imidazole **3** and the chloroimidazole **12** were included for comparison. In contrast to the 13-membered saturated linker, substitution at the  $\beta$ -position on the unsaturated linker did not improve FXIa affinity. The (*S*)- $\beta$ -Me **13** exhibited a 12-fold loss in FXIa affinity and the corresponding (*R*)- $\beta$ -Me **14**<sup>19</sup> was equipotent to the unsubstituted linker **3** and only slightly less active than the saturated linker (*S*)- $\beta$ -Me **9**. It should be noted that the configuration of the  $\beta$ -stereocenter is the same for both (*R*)- $\beta$ -Me **14** and (*S*)- $\beta$ -Me **9**. However the *S* designation changed to *R* based on the presence of the alkene in the macrocyclic linker which altered the prioritization in the Cahn-Ingold-Prelog system.

Substitution at the  $\alpha$ -position was explored next. Whereas the  $\alpha$ -Me **15** (diastereomer A) showed a modest loss in both FXIa affinity and aPTT activity compared to **3**, the corresponding  $\alpha$ -Me **16** (diastereomer B) led to a 16-fold loss in FXIa affinity and a 4-fold loss in activity in the aPTT clotting assay. In summary, alkyl substitution on the 13-membered unsaturated linker did not lead to an improvement in potency. Since potency enhancements were not seen, the corresponding chloroimidazoles analogs of **14** and **15** were not prepared.

**Table 3.** Substitutions on the 13-membered unsaturated macrocyclic linker



Compd #	R	X	FXIa $K_i$ (nM) <sup>12</sup>	aPTT $EC_{1.5x}$ ( $\mu$ M) <sup>13</sup>
<b>3</b>	H	H	0.16	0.27
<b>12</b>	H	Cl	0.03	0.28
<b>13</b> <sup>a</sup>	( <i>S</i> )- $\beta$ -Me <sup>b</sup>	H	2.0	0.98
<b>14</b> <sup>a</sup>	( <i>R</i> )- $\beta$ -Me <sup>b</sup>	H	0.13	0.38
<b>15</b> <sup>a</sup> (diastereomer A)	$\alpha$ -Me	H	0.33	0.67
<b>16</b> <sup>a</sup> (diastereomer B)	$\alpha$ -Me	H	2.7	1.2

<sup>a</sup>All diastereomers were separated following the ring-closing metathesis step. The diastereomeric excess of all final compounds was  $\geq$  95% de as determined by <sup>1</sup>H NMR. <sup>b</sup>The absolute stereochemistry was assigned based on an X-ray co-crystal of **14** with FXIa.

An X-ray crystal structure of compound **8** bound to human FXIa active site (2.1 Å resolution, Figure 2A) was obtained and revealed the absolute stereochemistry of the  $\beta$ -methyl to be in the *S*-configuration.<sup>18</sup> An overlay of compound **8** with the X-ray structure of compound **2** is shown in Figure 2B and highlights the interaction of the methyl group with the hydrophobic region (yellow surface) in the S1 prime pocket. Interestingly, an overlay of compound **8** and compound **14** (Figure 2C) suggests that the  $\beta$ -methyl in the unsaturated amide linker could still access the hydrophobic pocket. However this was not supported by the SAR described in Table 3 as **14** did not offer additional improvement in potency over **3**.

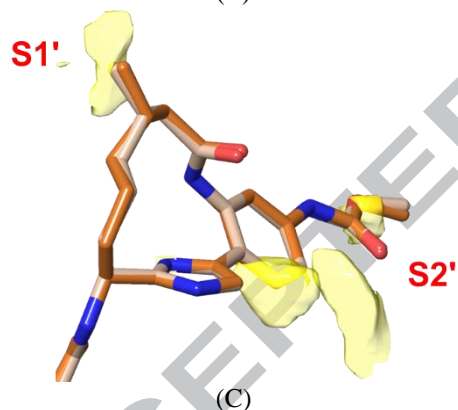
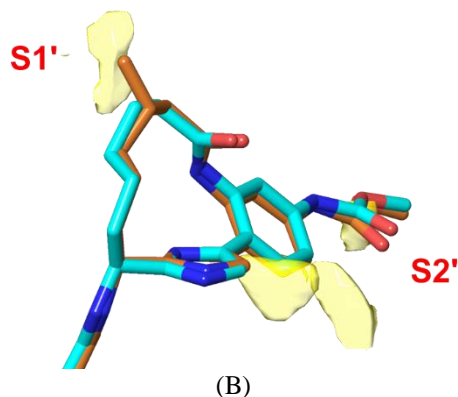
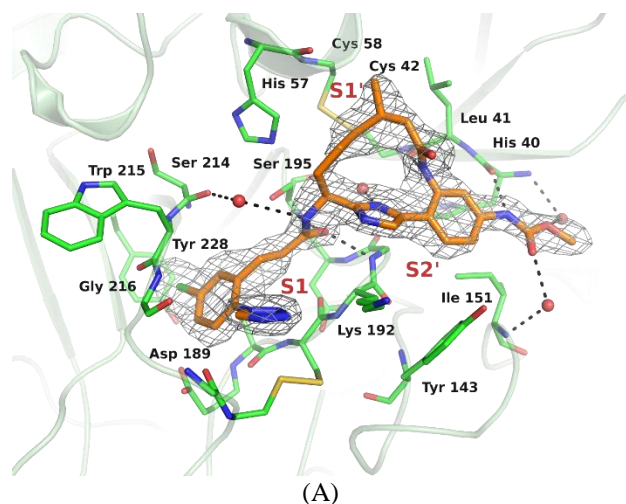


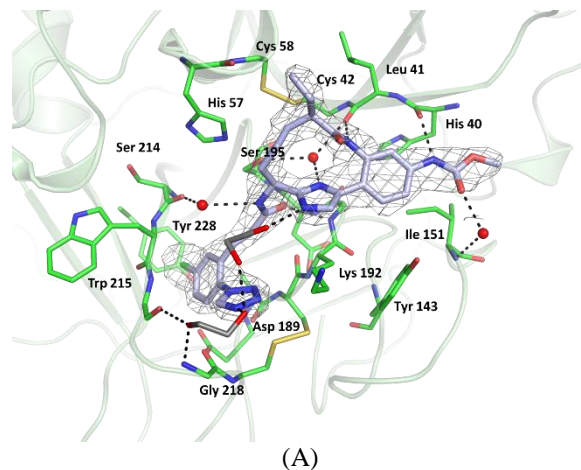
**Figure 2.** (A) X-ray crystal structure of 13-membered saturated macrocycle compound **8** bound to Factor XIa with omit electron density contoured at 3 rmsd (gray mesh). The red spheres depict water molecules and the dotted lines depict hydrogen bonds. (B) Overlay of X-ray crystal structures of **8** (orange) and **2** (cyan) in Factor XIa. (C) Overlay of X-ray crystal structures of **8** (orange) and **14** (wheat) in Factor XIa. Yellow surfaces highlight key hydrophobic regions within the FXIa binding site as determined by SiteMap.<sup>16</sup>

**Table 4.** Substitutions on the 12-membered saturated macrocyclic linker

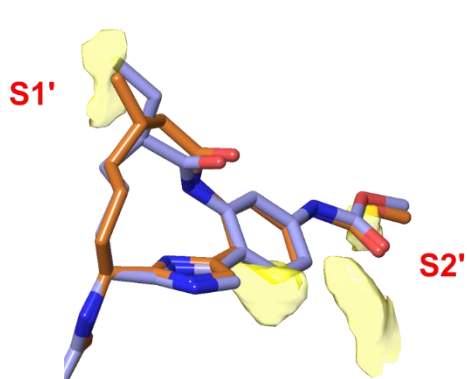
Compd #	R	X	FXIa Ki (nM) <sup>12</sup>	aPTT EC <sub>1.5x</sub> (μM) <sup>13</sup>
1	H	H	1.0	0.30
17 <sup>a</sup>	( <i>R</i> )-α-Me <sup>b</sup>	H	0.39	0.39
18	( <i>R</i> )-α-Me <sup>b</sup>	Cl	0.07	1.2
19	( <i>S</i> )-α-Me <sup>b</sup>	H	1.1	0.63
20	( <i>R</i> )-α-Et <sup>b</sup>	H	0.18	0.52
21	( <i>S</i> )-α-Et <sup>b</sup>	H	7.0	4.0
22	( <i>S</i> )-α-iPr <sup>c</sup>	H	0.14	1.1
23	( <i>R</i> )-α-iPr	H	21	64
24 <sup>d</sup>	β-Me	H	36	37
(diastereomer A)				
25 <sup>e</sup>	β-Me	H	35	31
(diastereomer B)				

<sup>a</sup>All diastereomers were separated. The diastereomeric excess of all final compounds was >95% de as determined by <sup>1</sup>H NMR. <sup>b</sup>The absolute stereochemistry was assigned based on X-ray co-crystals with FXIa. <sup>c</sup>The configuration of the α-stereocenter is the same as for (*R*)-α-Me **17** and (*R*)-α-Et **20**, however the *R* designation changed to *S* based on the iPr group which altered the prioritization in the Cahn-Ingold-Prelog system. <sup>d</sup>A 4:1 mixture of diastereomers. <sup>e</sup>A 2.6:1 mixture of diastereomers.

Since potency enhancements were achieved with β-substitution on the 13-membered saturated linker, we next explored substitutions on the 12-membered saturated linker (Table 4). In contrast to the saturated 13-membered macrocycle, addition of a methyl group at the β-position on the saturated 12-membered macrocycle resulted in over a 30-fold loss in FXIa affinity (**24** and **25** vs **1**). However, when the methyl group was introduced at the α-position, the (*R*)-isomer **17** improved FXIa affinity by 2-fold while the (*S*)-isomer **19** did not have a significant impact on FXIa affinity. Incorporation of the (*R*)-α-Me group in chloroimidazole **18** further improved FXIa Ki by 5-fold to 70 pM, albeit with a 3-fold loss in potency in the aPTT clotting assay (compare **17** and **18**). The 12-membered macrocycle (*R*)-α-Me **18** was equipotent to the 13-membered macrocycle (*S*)-β-Me **9**. Furthermore, as the size of the α-alkyl groups increased from methyl (**17**) to ethyl (**20**) to isopropyl (**22**), the FXIa affinity also improved stepwise from 0.4 nM to 0.2 nM and 0.1 nM. However, despite these potency enhancements with the larger alkyl group, a loss in aPTT clotting activity was observed. Overall, substitution of small alkyl groups at the α-position of the saturated amide linker improved FXIa affinity in the 12-membered macrocycle.



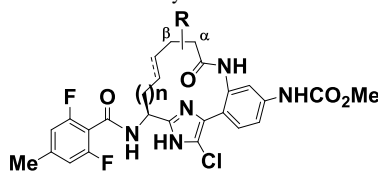
(A)



(B)

**Figure 3.** (A) X-ray crystal structure of 12-membered macrocycle compound **20** bound to Factor XIa with omit electron density contoured at 3 rmsd (gray mesh). The red spheres depict water molecules, the dotted lines depict hydrogen bonds, and ethylene diol is an artifact of the flash-cooling procedure. (B) Overlay of X-ray crystal structures of **20** (purple) and **8** (orange) in Factor XIa. Yellow surfaces highlight key hydrophobic regions within the FXIa binding site as determined by SiteMap.<sup>16</sup>

ACCEPTED MANUSCRIPT

**Table 5.** P1 modifications and rat PK for the 12- and 13-membered macrocycles

Compd #	n (ring size)	alkene	R	FXIa Ki (nM) <sup>12</sup>	aPTT EC <sub>1.5x</sub> (μM) <sup>13</sup>	Caco-2 AB/BA (nm/s)	PSA <sup>a</sup> (Å <sup>2</sup> )	HLM <sup>b</sup> T <sub>1/2</sub> (min)	Rat PK F% <sup>c</sup>
12 <sup>d</sup>	1 (13)	E-alkene	H	0.03	0.28	<15/58	169	58	0
26	0 (12)	saturated	(R)-α-Me	10	2.0	<15/111	125	8	NT <sup>e</sup>
27	1 (13)	saturated	(S)-β-Me	44	12	18/251	125	45	NT <sup>e</sup>
28	1 (13)	E-alkene	(R)-β-Me	12	2.7	<15/189	125	35	16
29	1 (13)	E-alkene	H	16	6.6	<15/200	125	17	41

<sup>a</sup>PSA = polar surface area. <sup>b</sup>HLM = human liver microsome stability. <sup>c</sup>Compounds were dosed in rat in an N-in-1 format.<sup>23</sup> Vehicle for both iv and po: 70% PEG400; 20% water; 10% ethanol. <sup>d</sup>Compound **12** contains the chlorophenyltetrazole cinnamide P1 and was included for comparison. <sup>e</sup>NT = not tested.

An X-ray crystal structure of **20** bound to human FXIa active site (2.6 Å resolution, Figure 3A) was obtained and revealed the absolute stereochemistry of the α-ethyl in the 12-membered macrocycle to be the *R*-configuration (the absolute stereochemistry of the α-methyl and α-*i*Pr were also confirmed by x-ray structures).<sup>20</sup> Interestingly, the (*R*)-stereochemistry is the opposite stereochemistry compared to the (*S*)-β-Me **8** in the saturated 13-membered macrocycle. An overlay of compound **20** and compound **8** is shown in Figure 3B and highlights the interaction of the alkyl groups with the hydrophobic region (yellow surface) in the S1 prime pocket. Despite the differences in both the position of substitution and the stereochemistry, the (*S*)-β-Me **8** on the 13-membered saturated amide linker and the (*R*)-α-Et **20** on the 12-membered saturated amide linker are able to access the same hydrophobic region near the S1 prime pocket.

Multiple alkyl-substituted macrocycles, (*S*)-β-Me **9**, (*R*)-β-Me **14**, and (*R*)-α-Me **18**, were identified that exhibited exquisite FXIa affinity and were comparable to the unsubstituted 13-membered macrocycle **12**. With potent macrocycles in hand, we next sought to address the poor oral bioavailability for the series which we attributed to low permeability arising from high polar surface area (PSA).<sup>14</sup> For example, unsubstituted 13-membered macrocycle **12** exhibited poor Caco-2 permeability (A to B/B to A < 15/58 nm/sec) and a high PSA (169 Å<sup>2</sup>), and was found to not have oral bioavailability in rat. Since the chlorophenyltetrazole cinnamide P1 was a major contributor to high PSA, new P1 groups with lower PSA values were desired. Previously we had shown that oral bioavailability could be achieved in our linear series of FXIa inhibitors with less polar benzamide P1 groups.<sup>21</sup> As a result, the macrocycles from **18**, **9**, **14**, and **12** were combined with 2,6-difluoro-4-methyl benzamide (Table 5). Replacing chlorophenyltetrazole cinnamide in the 12-membered macrocycle **18** with benzamide gave **26**, which resulted in a significant loss (>140-fold) in FXIa affinity but only a modest loss in potency in the aPTT clotting assay. Installation of benzamide in the 13-membered saturated macrocycle led to **27** with an even greater loss (>700-fold) in FXIa affinity. Interestingly, even though the 13-membered macrocycle **9** and 12-membered macrocycle **18** both containing the chlorophenyltetrazole cinnamide were comparable in FXIa affinity, when combined with the

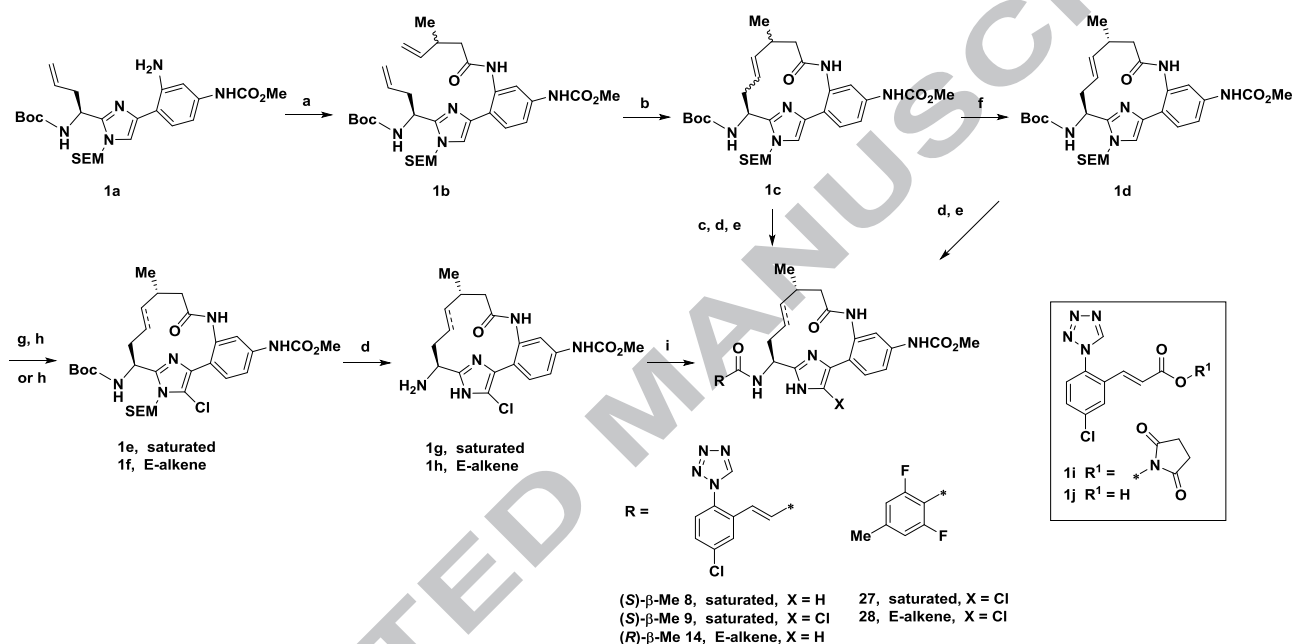
smaller benzamide, the 12-membered macrocycle was more potent (**26** vs **27**). The 13-membered macrocycles **28** and **29**, possessing the E-alkene, were comparable to **26**. The loss in potency with the smaller benzamide P1 can be explained by the fact that the phenyl moiety does not extend as deep into the S1 pocket and cannot engage key residues as was seen with the larger chlorophenyltetrazole P1.<sup>22</sup> Even though replacement of the chlorophenyltetrazole cinnamide resulted in a significant loss in FXIa affinity, these analogs (**26-29**) have a lower PSA as shown in Table 5. Permeability for this set of macrocycles was improved compared to **12** based on the Caco-2 B to A permeability; however the efflux ratio was very high. Macrocyclic compounds **28** and **29** were evaluated in a rat pharmacokinetic model, using an N-in-one cassette dosing protocol<sup>23</sup> (Table 5). Replacing the chlorophenyltetrazole with 2,6-difluoro-4-methyl benzamide resulted in compounds with low clearance, short half-life, and improved oral bioavailability (%F = 16 - 41). (Please see Supplementary Data for detailed pharmacokinetic data)

The synthesis of the β-methyl substituted 13-membered macrocycles are described in Scheme 1. For the 13-membered macrocycles the key macrocyclization step utilized a ring-closing olefin metathesis (RCM) strategy.<sup>24</sup> Aniline **1a**<sup>11</sup> was coupled with 3-methylpent-4-enoic acid using T3P which gave amide **1b** as a mixture of diastereomers. Amide **1b** was pretreated with *p*-TsOH to form the imidazolium ion and then cyclized via RCM using the 2<sup>nd</sup> generation Grubbs II catalyst which gave the 13-membered macrocycle **1c** as a mixture of E and Z-alkene isomers as well as a mixture of (*R*)- and (*S*)-stereoisomers.<sup>25</sup> Hydrogenation of **1c** over palladium on carbon, followed by deprotection with 4M HCl at elevated temperature afforded the corresponding amine as a mixture of diastereomers. Chlorophenyltetrazole cinnamide was installed by coupling amine with activated carboxylic ester **1i** which gave, following separation of diastereomers by chiral preparatory hplc, (*R*)-β-Me **7** (not shown) and (*S*)-β-Me **8**. Alternatively, the stereoisomers can be separated by reverse phase preparatory hplc following the RCM step which gave **1d**. Hydrogenation of **1d** over palladium on carbon, followed by chlorination of the imidazole with N-chlorosuccinimide at elevated temperature provided chloroimidazole **1e**. Global deprotection as described above

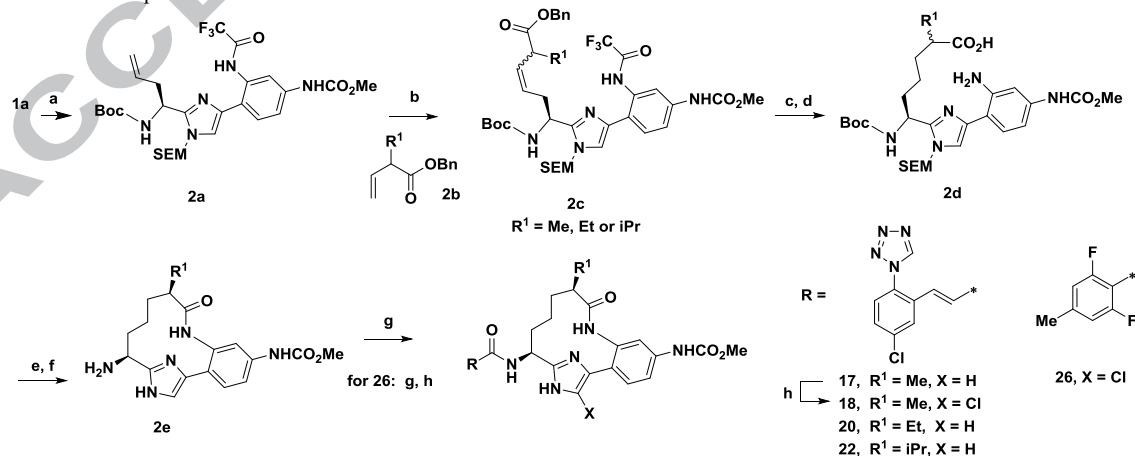
provided amine **1g**, which was then coupled with the appropriately substituted carboxylic acids to give **9** and **27**. Analogs **14** and **28** were prepared following the sequence described above. The  $\alpha$ - and  $\gamma$ -methyl substituted 13-membered macrocycle analogs were prepared as described above by replacing 3-methylpent-4-enoic acid with 2-methylpent-4-enoic acid and 4-methylpent-4-enoic acid, respectively.

The synthesis of the  $\alpha$ -alkyl substituted 12-membered macrocycles is described in Scheme 2. In contrast to the 13-membered ring macrocycles described above, the 12-membered macrocycles were prepared via a key macrolactamization step. Aniline **1a** was protected as trifluoroacetamide **2a**. Intermolecular metathesis of **2a** with the benzyl ester of  $\alpha$ -substituted butenoic acids **2b** using 2<sup>nd</sup>

generation Grubbs II catalyst provided compounds **2c**. Hydrogenation of **2c** simultaneously reduced the double bond and deprotected the benzyl ester, which upon hydrolysis of the trifluoroacetamide gave acid anilines **2d**. Macrolactamization of **2d** under dilute coupling conditions with BOP and DMAP afforded the desired 12-membered macrocycles as a mixture of diastereomers which were separated by reverse phase preparatory hplc. Deprotection and installation of the P1 groups as described in Scheme 1 provided analogs **17**, **20**, and **22**. Analog **18** was obtained by chlorination of **17** and intermediate **2e** was converted to **26** following a similar sequence. The  $\beta$ -methyl substituted 12-membered amide-linked analogs were prepared as described above by replacing the benzyl ester of  $\alpha$ -substituted butenoic acids **2b** with benzyl 3-methylbut-3-enoate.



**Scheme 1.** Reagents and conditions: (a) 3-methylpent-4-enoic acid, T3P, Hunig's base, EtOAc, -10 °C to rt, 95%; (b) Second generation Grubbs II catalyst (40 mol%), *p*TsOH, DCM, reflux, 68%; (c) 10% Pd/C, H<sub>2</sub>, MeOH; (d) 4M HCl in dioxane, 50 °C or 75 °C, 55% over two steps; (e) **1i**, Hunig's base, DMF, 55%, then chiral preparatory hplc to separate diastereomers; (f) reverse phase chromatography to separate diastereomers, 10%; (g) 10% Pd/C, H<sub>2</sub> (55 psi), EtOH, 78%; (h) NCS, ACN, CHCl<sub>3</sub>, 65 °C, 35-55%; (i) **1j** or 2,6-difluoro-4-methylbenzoic acid, EDC, HOBT, Hunig's base or triethylamine, DMF, 32-44% over two steps.



**Scheme 2.** Reagents and conditions: (a) 2,2,2-trifluoroacetic anhydride, triethylamine, EtOAc, 0 °C 97%; (b) Second generation Grubbs II catalyst (40 mol%), *p*TsOH, DCM, reflux or microwave 150 °C, 18-49%; (c) 10% Pd/C, H<sub>2</sub>, MeOH, 69-100%; (d) LiOH, MeOH, 60 °C, 74-100%; (e) BOP, DMAP,

DIEA, DMF/DCM, then reverse phase HPLC separation of diastereomers, 15-35%; (f) 4M HCl in dioxane, 50 °C, 100%; (g) **1i**, Hunig's base, DMF, 48-73% or 2,6-difluoro-4-methylbenzoic acid, EDC, HOBT, Hunig's base or triethylamine, DMF; (h) NCS, ACN, CHCl<sub>3</sub>, 65 °C, 35-55%.

ACCEPTED MANUSCRIPT

In conclusion, the macrocyclic FXIa series described herein was optimized by modifying both the macrocyclic linker and the P1 group. SAR exploration of macrocyclic linker identified key alkyl substitutions which improved FXIa affinity by interacting with a hydrophobic region near the S1 prime pocket as demonstrated by ligand bound X-ray crystal structures. Both the position of substitution and the absolute stereochemistry of the alkyl moiety on the macrocyclic linker varied with the size of the macrocyclic ring. The (*S*)- $\beta$ -Me group was more potent in the 13-membered saturated linker while the (*R*)- $\alpha$ -Me moiety was more potent in the 12-membered saturated linker. Replacement of the P1 group, chlorophenyltetrazole cinnamide, was a successful approach for reducing the PSA and improving the oral bioavailability for the macrocyclic series. However, this P1 modification came with a loss in potency. Further optimization of the P1 to improve FXIa potency and maintain the oral bioavailability will be reported in due course.

**Acknowledgements:** The authors thank the Department of Discovery Synthesis for the synthesis of intermediates at BMS Biocon Research Center; the Department of Lead Discovery & Optimization; and Mojgan Abousleiman for in vitro work.

#### A. Supplementary Data.

Supplementary data associated with this article can be found, in the online version, at <http://dx.doi.org/>

#### References and Notes

- (a) Morais, J.; De Caterina, R. *Cardiovasc. Drugs Ther.* **2016**, *30*, 201-214. (b) Schaefer, J. K.; McBane, R. D.; Wysokinski, W. E. *Ann. Hematol.* **2016**, *95*, 437. (c) Levy, J. H.; Spyropoulos, A. C.; Samama, C. M.; Douketis, J. *J. Am. Coll. Cardiol. Intv.* **2014**, *7*, 1333.
- Gulpen, A. J. W.; Cate-Hoek, A. J. T.; Cate, H. T. *Expert Review of Cardiovascular Therapy*, **2016**.
- In 2013 the European Union approved rivaroxaban for secondary prevention in ACS despite an increased risk of bleeding and intracranial hemorrhage. Please see (a) Behnes, M.; Fastner, C.; Ansari, U.; Akin, I. *Cardiovasc. Hematol. Disord.: Drug Targets* **2015**, *15*, 101. (b) Oldgren, J.; Wallentin, L.; Alexander, J. H.; James, S.; Jonelid, B.; Steg, G.; Sundstrom, J. *Eur. Heart J.* **2013**, *34*, 1670.
- (a) Bane, C. E.; Gailani, D. *Drug Discovery Today* **2014**, *19* (9), 1454. (b) Muller, F.; Gailani, D.; Renne, T. *Curr. Opin. Hematol.* **2011**, *18*, 349.
- (a) Salomon, O.; Steinberg, D. M.; Koren-Morag, N.; Tanne, D.; Seligsohn, U. *Blood* **2008**, *111* (8), 4113. (b) Salomon, O.; Steinberg, D. M.; Zucker, M.; Varon, D.; Zivelin, A.; Seligsohn, U. *Thromb. Haemost.* **2011**, *105*, 269.
- Bane, C. E.; Neff, A. T.; Gailani, D. Factor XI deficiency or hemophilia C. In *Hemostasis and Thrombosis: Practical Guidelines in Clinical Management*; Saba, H.I., Roberts, H. R., Eds.; John Wiley & Sons, Ltd.: Oxford, 2014; pp 71-81.
- Lin, J.; Deng, H.; Jin, L.; Pandey, P.; Quinn, J.; Cantin, S.; Rynkiewicz, M. J.; Gorga, J. C.; Bibbins, F.; Celatka, C. A.; Nagafuji, P.; Bannister, T. D.; Meyers, H. V.; Babine, R. E.; Hayward, N. J.; Weaver, D.; Benjamin, H.; Stassen, F.; Abdel-Meguid, S. S.; Strickler, J. E. *J. Med. Chem.* **2006**, *49*, 7781.
- (a) Schumacher, W. A.; Seiler, S. E.; Steinbacher, T. E.; Stewart, A. B.; Bostwick, J. S.; Hartl, K. S.; Liu, E. C.; Ogletree, M.L. *Eur. J. Pharmacol.* **2007**, *570*, 167. (b) Wong, P. C.; Crain, E. J.; Watson, C. A.; Schumacher, W. A. *J. Thromb. Thrombolysis* **2011**, *32*, 129.
- (a) Quan, M. L.; Wong, P. C.; Wang, C.; Woerner, F.; Smallheer, J. M.; Barbera, F. A.; Bozarth, J. M.; Brown, R. L.; Harpel, M. R.; Luetzgen, J. M.; Morin, P. E.; Peterson, T.; Ramamurthy, V.; Rendina, A. R.; Rossi, K. A.; Watson, C. A.; Wei, A.; Zhang, G.; Seiffert, D.; Wexler, R. R. *J. Med. Chem.* **2014**, *57*(3), 955. (b) Wong, P. C.; Quan, M. L.; Watson, C. A.; Crain, E. J.; Harpel, M. R.; Rendina, A. R.; Luetzgen, J. M.; Wexler, R. R.; Schumacher, W. A.; Seiffert, D. A. *J. Thromb. Thrombolysis* **2015**, *40*(4), 416.
- Hu, Z.; Wong, P. C.; Gilligan, P. J.; Han, W.; Pabbisetty, K. B.; Bozarth, J. M.; Crain, E. J.; Harper, T.; Luetzgen, J. M.; Myers, J. E.; Ramamurthy, V.; Rossi, K. A.; Sheriff, S.; Watson, C. A.; Wei, A.; Zheng, J. J.; Seiffert, D. A.; Wexler, R. R.; Quan, M. L. *ACS Med. Chem. Lett.* **2015**, *6*, 590.
- Corte, J. R.; Fang, T.; Osuna, H.; Pinto, D. J. P.; Rossi, K. A.; Myers, J. E.; Sheriff, S.; Lou, Z.; Zheng, J. J.; Harper, T. W.; Bozarth, J. M.; Wu, Y.; Luetzgen, J. M.; Seiffert, D. A.; Decicco, C. P.; Wexler, R. R.; Quan, M. L. *J. Med. Chem.* **2017**, *60*, 1060.
- Ki values were obtained from purified human enzyme at 37 °C and were averaged from multiple determinations (n=2), as described in Refs. 9b and 11.
- aPTT (activated partial thromboplastin time) in vitro clotting assay was performed in human plasma as described in Refs. 9b and 11. The reported EC<sub>1,5x</sub> values are the FXIa inhibitor plasma concentrations which produce a 50% increase in the clotting time relative to the clotting time in the absence of the inhibitor.
- Ertl, P. Polar Surface Area. In *Molecular Drug Properties. Measurement and Prediction*; Mannhold, R., Ed.; Wiley-VCH Verlag GmbH & Co. KGaA: Weinheim, 2008; pp 111-126.
- PDB deposition number for **1** is 5Q0D.
- The yellow surfaces highlight key hydrophobic regions within the FXIa binding site as determined by SiteMap, please see Halgreen, T. *Chem. Biol. Drug Des.* **2007**, *69*, 146.
- Hangeland, J. J.; Friends, T. J.; Rossi, K. A.; Smallheer, J. M.; Wang, C.; Sun, Z.; Corte, J. R.; Fang, T.; Wong, P. C.; Rendina, A. R.; Barbera, F. A.; Bozarth, J. M.; Luetzgen, J. M.; Watson, C. A.; Zhang, G.; Wei, A.; Ramamurthy, V.; Morin, P. E.; Bisacchi, G. S.; Subramaniam, S.; Arunachalam, P.; Mathur, A.; Seiffert, D. A.; Wexler, R. R.; Quan, M. L. *J. Med. Chem.* **2014**, *57*, 9915.
- The absolute stereochemistry was assigned based on an X-ray co-crystal of (*S*)- $\beta$ -Me **8** with FXIa (Figure 2A). The PDB deposition number for (*S*)- $\beta$ -Me **8** is 5Q0E.
- The absolute stereochemistry was assigned based on an X-ray co-crystal of (*R*)- $\beta$ -Me **14** with FXIa. The PDB deposition number for (*R*)- $\beta$ -Me **14** is 5Q0F.
- The absolute stereochemistry was assigned based on an X-ray co-crystal of (*R*)- $\alpha$ -Et **20** with FXIa. The PDB deposition number for (*R*)- $\alpha$ -Et **20** is 5Q0G.
- Pinto, D. J. P.; Smallheer, J. M.; Corte, J. R.; Austin, E. J. D.; Wang, C.; Fang, T.; Smith, L. M.; Rossi, K. A.; Rendina, A. R.; Bozarth, J. M.; Zhang, G.; Wei, A.; Ramamurthy, V.; Sheriff, S.; Myers, J. E.; Morin, P. E.; Luetzgen, J. M.; Seiffert, D. A.; Quan, M. L.; Wexler, R. R. *Bioorg. Med. Chem. Lett.* **2015**, *25*, 1635.
- For the chlorophenyltetrazole cinnamide P1: The chlorophenyl portion fills the S1 pocket with the chlorine atom forming a  $\pi$ -Cl interaction with Tyr228; the tetrazole portion extends out of the S1 pocket and interacts with the Cys191-Cys219 disulfide bridge; and the tetrazole N4 nitrogen forms an H-bond, via a series of water molecules, to Gly218. The smaller benzamide P1 does not interact with these key residues. Please see Supplementary data for an overlay of compounds **28** and **14**.
- He, K.; Qian, M.; Wong, H.; Bai, S. A.; He, B.; Brogdon, B.; Grace, J. E.; Xin, B.; Wu, J.; Ren, S. X.; Zeng, H.; Deng, Y.; Graden, D. M.; Olah, T. V.; Unger, S. E.; Luetzgen, J. M.; Knabb, R. M.; Pinto, D. J.; Lam, P. Y. S.; Duan, J.; Wexler, R. R.; Decicco, C. P.; Christ, D. D.; Grossman, S. J. *J. Pharm. Sci.* **2008**, *97* (7), 2568.
- Van Lierop, B. J.; Lummiss, J. A. M.; Fogg, D. E. Ring-closing metathesis. In *Olefin Metathesis: Theory and Practice*; Grela, K., Ed.; John Wiley & Sons Inc.: Hoboken, New Jersey, 2014; pp 85-152.
- Chen, Y.; Dias, H. V. R.; Lovely, C. J. *Tetrahedron Lett.* **2003**, *44*, 1379.

## Graphical Abstract

**Macrocyclic Inhibitors of Factor XIa:  
Discovery of Alkyl-Substituted Macrocyclic  
Amide Linkers with Improved Potency.**

James R. Corte\*, Wu Yang\*, Tianan Fang, Yufeng Wang, Honey Osuna, Amy Lai, William R. Ewing, Karen A. Rossi, Joseph E. Myers Jr., Steven Sheriff, Zhen Lou, Joanna J. Zheng, Timothy W. Harper, Jeffrey M. Bozarth, Yiming Wu, Joseph M. Luetzgen, Dietmar A. Seiffert, Mimi L. Quan, Patrick Y. S. Lam, and Ruth R. Wexler

